(Preprint) AAS 21-698

GEOMETRIC APPROACH TO THE DESIGN OF LUNAR-GRAVITY-ASSISTED LOW-ENERGY EARTH-MOON TRANSFERS

Anastasia Tselousova,[*] Sergey Trofimov,[†] Maksim Shirobokov,[‡] and Denis Perepukhov[§¶]

Based on the previously obtained database of planar ballistic lunar transfer trajectories in the bicircular four-body problem (BR4BP) model, we apply several conventional analytical tools for the design of high-energy gravity-assist maneuvers in order to map the required (i.e., corresponding to a certain ballistic transfer) conditions on the boundary of the region of prevalence (an analog of the sphere of influence concept in the BR4BP) to the parking orbit departure parameters providing an intermediate lunar flyby to achieve such conditions. Obtained analytical estimates enable avoiding dependence on a specific near-Earth parking orbit in the early stages of mission design and represent the departure parameters corresponding to lunar-gravity-assisted ballistic transfer trajectories within the framework of the patched conic approximation model. These parameters are subsequently refined when adapting a trajectory to more complex models of motion by the multiple-shooting procedure.

INTRODUCTION

In recent years, much attention has been paid to the exploration of the Moon and circumlunar space. In particular, all the world's major space agencies are jointly involved in the development of a habitable lunar orbital station called the Lunar Orbital Platform-Gateway (LOP-G).[1] In this context, the issue of searching for fuel-efficient transfers to transport materials to circumlunar orbits has become a topic of increasing attention. One of the most attractive transportation options are low-energy trajectories. It is a class of efficient transfer trajectories characterized by the property of *ballistic capture* when the spacecraft's Keplerian energy with respect to the Moon becomes negative from initially positive values without an additional impulse. Ballistic capture is temporary and is also referred to as weak. Compared to traditional high-energy transfers with the injection and final orbit insertion impulsive maneuvers, low-energy trajectories provide considerable fuel savings and larger launch windows, although the time of flight is significantly increased. Charles Conley was

[*]Junior Researcher, Space Systems Dynamics Department, Keldysh Institute of Applied Mathematics, 4 Miusskaya Sq., 125047 Moscow, Russia

[†]Senior Researcher, Space Systems Dynamics Department, Keldysh Institute of Applied Mathematics, 4 Miusskaya Pl., 125047 Moscow, Russia

[‡]Senior Researcher, Space Systems Dynamics Department, Keldysh Institute of Applied Mathematics, 4 Miusskaya Pl., 125047 Moscow, Russia

[§]Senior Engineer, Laboratory of Intelligent Information Systems, Keldysh Institute of Applied Mathematics, 4 Miusskaya Pl., 125047 Moscow, Russia

[¶]Master Student, Phystech school of Applied Mathematics and Informatics, Moscow Institute of Physics and Technology, 9 Institutskiy Per., 141701 Dolgoprudny, Moscow Region, Russia

the first to rigorously prove the existence of low-energy transfers in the frame of circular restricted three-body problem model and revealed the effect of ballistic capture.[2] The term ballistic capture was, however, coined later by Edward Belbruno.[3] Subsequently, various numerical methods of low-energy Earth-Moon trajectories design have been developed based on the dynamical properties of the three- and four-body systems.[4–11]

Low-energy Earth-Moon transfer trajectories that benefit from the Sun's gravitational perturbation are called *weak stability boundary* (WSB) trajectories or *ballistic lunar transfers* (BLT). When designed with the proper geometry, a WSB trajectory first departs far away from the Earth-Moon system, where the solar gravity pulls its perigee from the altitude of the initial near-Earth parking orbit up to the radius of the Moon's orbit, and then, a spacecraft heads toward the Moon to be captured ballistically. Such transfers were used in the Hiten[12] (JAXA, 1991) and GRAIL[13] (NASA, 2011) missions. According to a recent study, WSB trajectories have the maximum fuel efficiency among two-impulse transfers in the Earth-Moon-Sun planar bicircular four-boby problem (BR4BP) model, especially with lunar flybys included.[14] A lunar flyby in that case allows reducing the launch energy C_3 and the transfer delta-v cost, along with assisting in the change of the inclination if required.[15]

Existing methods of designing lunar-gravity-assisted WSB transfers rely on numerical optimization techniques without intentionally targeting a certain flyby.[14–18] At the same time, there are several conventional analytical tools for the high-energy gravity assist analysis in the framework of the patched conics model that could potentially be applied to the design of an intermediate high-energy lunar flyby along low-energy trajectories. First, the *B-plane* can be mentioned. It is a plane passing through the gravity-assist body center perpendicular to the asymptote of the incoming hyperbolic trajectory.[19] The coordinates on the plane uniquely determine the lunar flyby parameters and the subsequent trajectory around the central body; therefore, the B-plane points can be targeted on the preliminary stages of the gravity assist design.[20] A useful tool for the design of near-coplanar multiple gravity-assist trajectories is the *Tisserand graph*. This graph represents the v_∞ contours on the plane of the orbital parameters (e.g., the orbital period vs. the periapse distance) with respect to the central body.[21] Each point on the plot corresponds to an orbit around the central body, and that orbit can be modified by flying by some celestial body orbiting the central one while moving along the corresponding v_∞ contour.[21] When designing non-coplanar gravity-assist maneuvers, the v_∞ *globe* is especially valuable. It is a sphere formed by all the $\mathbf{v}_\infty$ vectors of the same magnitude. Thus, the points on the surface of the v_∞ globe correspond to all possible incoming/outgoing hyperbolas with a given v_∞ magnitude.[22] To target specific geocentric parameters (the orbital period, the inclination, etc.) after a lunar flyby, it is convenient to draw contour lines on the v_∞ globe or its map projection.[23]

This work is aimed at incorporating similar analytical tools in the design and analysis of low-energy trajectories with lunar flybys in the planar BR4BP model. Using the analytical formulas from the patched conic approximation model and the previously obtained dataset of planar lunar-gravity-assisted WSB transfers in the BR4BP model of motion,[24] the authors analytically estimate the departure parameters that ensure a lunar flyby providing a desired WSB transfer. For this, we map the characteristics of the desired WSB trajectories on the boundary of the region of prevalence[25] (an analog of the sphere of influence concept in the BR4BP model) and target them. These parameters are subsequently refined when adapting the trajectory to more complex models of motion by the multiple-shooting procedure.

The structure of the paper is as follows. First, we outline the models of motion used. Then the brief description of the numerical algorithm for the design of planar WSB transfers in the BR4BP model is presented. After that, we analyze the properties of lunar-gravity-assisted WSB transfers obtained in the planar BR4BP and give a description of the targeting algorithm. As an example, we consider WSB transfers from the 200 km circular near-Earth parking orbit to the near-Moon orbits of the same size as the near-rectilinear resonant halo orbit 9:2, the main candidate for the location of the LOP-G. Then the accuracy of the presented targeting algorithm is examined.

DYNAMICAL MODELS

Patched Conic Approximation

The patched conic approximation is one of the simplest analytical models when designing trajectories in a multiple-body environment. Within the framework of this model, at each moment of time, the spacecraft moves under the central gravitational field of only one primary, which corresponds to the classical two-body problem model. In this case, to define the dominant gravitating body, the concept of the *sphere of influence* (SOI)[26] is used. For the Earth-Moon system, it is a closed surface that limits the volume around the Moon, where the ratio of gravitational perturbation from the Earth to the Moon's gravity (if the Moon is considered as the central body) is less than the ratio of gravitational perturbation from the Moon to the Earth's gravity (here the Earth is defined as the central body). The boundary of the volume is approximated by a sphere with a radius

$$r_{SOI} = R_M(m_M/m_E)^{2/5} \approx 66194 \text{ km}.$$

We denote by m_E and m_M the masses of the Earth and the Moon, respectively; R_M is the mean radius of the Moon. Thus, according to the patched conic approximation, inside the SOI, the Moon is considered as the primary in the two-body problem model, whereas outside the SOI, the Earth plays this role. When crossing the boundary of the SOI, the primary changes and the spacecraft's relative positions and velocities are recalculated.

Circular Restricted Three-body Problem

The circular restricted three-body problem (CR3BP) model is dynamically more complex than the patched conic approximation. The CR3BP assumes that at any time the spacecraft moves simultaneously in the central gravitational fields of two primaries, the Earth and the Moon in our case. The spacecraft is considered to be of negligible mass; the Earth and the Moon revolve in circular orbits around their center of mass C. It is convenient to write the equations of motion of the CR3BP in the standard rotating coordinate frame (see Figure 1, a) with the origin at C, the x-axis connecting the masses m_E and m_M towards m_M, the z-axis directed along the angular velocity of the orbital motion of m_M around m_E, and the y-axis completing the right-handed system.

It is also convenient to use a dimensionless system of units in which 1) masses are normalized so that $m_E = 1 - \mu$ and $m_M = \mu$ where $\mu = m_M/(m_E + m_M)$, 2) the angular velocity of the rotating frame is normalized to one, and 3) the distance between m_E and m_M is normalized to one. Thus, the dimensionless universal gravitational constant G is also identically equal to one. For the Earth-Moon system, the corresponding units of distance, velocity and time are the following:

$$\begin{aligned} \text{DU} &= 384402 \text{ km}, \\ \text{VU} &= 1.024544182251307 \text{ km/s}, \\ \text{TU} &= 4.342513772754916 \text{ days}, \end{aligned} \tag{1}$$

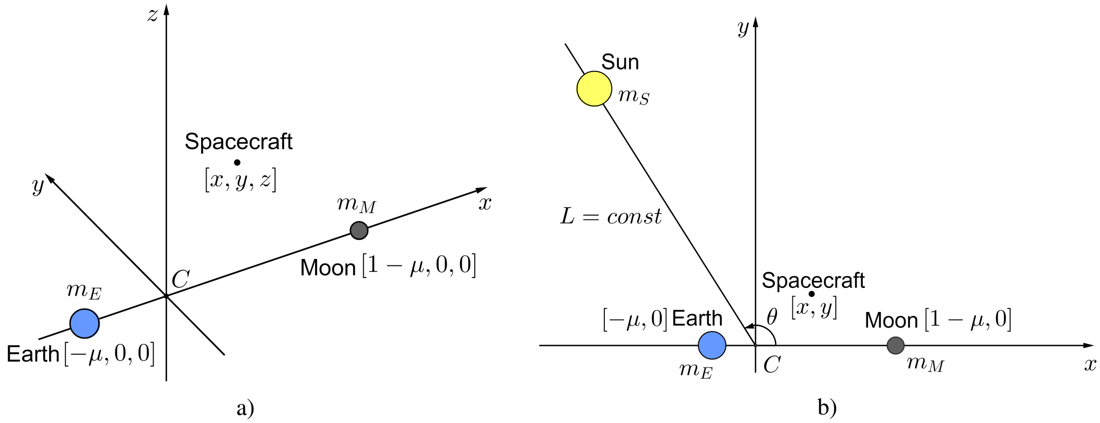

Figure 1. Rotating reference frames in the Earth-Moon circular restricted three-body problem (a) and the Earth-Moon-Sun planar bicircular four-body problem (b).

and the mass parameter $\mu = 0.012150584460351$. In this system of units, m_E and m_M are at fixed positions at $[-\mu, 0, 0]$ and $[1-\mu, 0, 0]$ along the x-axis, respectively. The equations of motion are expressed in the nondimensional form as

$$\ddot{x} - 2\dot{y} = \frac{\partial \Omega_3}{\partial x}, \quad \ddot{y} + 2\dot{x} = \frac{\partial \Omega_3}{\partial y}, \quad \ddot{z} = \frac{\partial \Omega_3}{\partial z}, \tag{2}$$

where

$$\Omega_3(x, y, z) = \frac{x^2 + y^2}{2} + \frac{1-\mu}{r_1} + \frac{\mu}{r_2} + \frac{\mu(1-\mu)}{2}$$

is the effective potential. The distances to m_E and m_M are given by the equalities

$$r_1^2 = (x+\mu)^2 + y^2 + z^2,$$

$$r_2^2 = (x-1+\mu)^2 + y^2 + z^2.$$

The system (2) has an integral of motion, the Jacobi integral,

$$J(x, y, z, \dot{x}, \dot{y}, \dot{z}) = 2\Omega_3(x, y, z) - (\dot{x}^2 + \dot{y}^2 + \dot{z}^2),$$

and, thus, all the solutions of Eq. (2) at any time lie on the manifold $\mathcal{J}(J_{EM}) = \{[x, y, z, \dot{x}, \dot{y}, \dot{z}] \in \mathbb{R}^6 | J(x, y, z, \dot{x}, \dot{y}, \dot{z}) = J_{EM}\}$ for some energy level J_{EM}. A planar motion can be obtained by setting $z \equiv 0$.

Bicircular Restricted Four-Body Problem

The bicircular restricted four-body problem incorporates the perturbation of the third primary. When constructing Earth-Moon WSB transfers, the gravitational perturbations from the Sun play a key role. Thus, in this context, it is reasonable to consider the Earth-Moon-Sun BR4BP. The Sun is assumed to revolve in a circular orbit of radius $L \gg 1$ around the Earth-Moon center of mass in the same plane (see Figure 1, b). The direction to the Sun in the CR3BP rotating reference frame is determined by θ — the phase of the Sun.

In order to obtain the BR4BP equations of motion in the nondimentional form from the CR3BP ones, it is enough to replace the effective potential by

$$\Omega_4(x,y,z) = \Omega_3(x,y,z) + \Omega_{4b}(x,y,z,t) = \Omega_3(x,y,z) + \frac{Gm_S}{r_3(t)} - \frac{Gm_S}{L^2}(x\cos\theta(t) + y\sin\theta(t)),$$

where $r_3(t) = \sqrt{(x - L\cos\theta(t))^2 + (y - L\sin\theta(t))^2 + z^2}$ is the distance from the spacecraft to the Sun, $Gm_S = 3.289005596145305 \times 10^5$ is the dimensionless gravitational parameter of the Sun, and the phase of the Sun linearly grows over time:

$$\theta(t) = \theta_0 + w_S(t - t_0). \tag{3}$$

For $L = 389.17$, which corresponds to 1 astronomical unit, the orbital velocity of the Sun is determined as follows: $w_S = \sqrt{\frac{1+m_S}{L^3}} - 1 \approx -0.9253$.

A planar case of BR4BP is obtained when $z \equiv 0$.

Earth-Moon Region of Prevalence

By analogy with the patched conic approximation, it is possible to specify a volume around the Earth-Moon system in the framework of the BR4BP model where the Sun's gravitational perturbation can be neglected and the Earth-Moon CR3BP is accurate to model the spacecraft's motion. In a planar case, for this purpose, the concept of the *region of prevalence* (RoP) can be used.[25] According to Castelli, the boundary of the Earth-Moon RoP consists of points in the configuration space where the error in the right-hand side of the spacecraft's equations of motion would have the same magnitude independently of what body–the Moon or the Sun–we neglect in the Earth-Moon-Sun system.

Although the boundary of the RoP depends on the value of the phase of the Sun θ, it can be mean-square approximated by an ellipse in the Earth-Moon rotating reference frame (see Figure 2). In Figure 2 the boundaries of the Earth-Moon RoP, depending on θ, are shown by colored closed

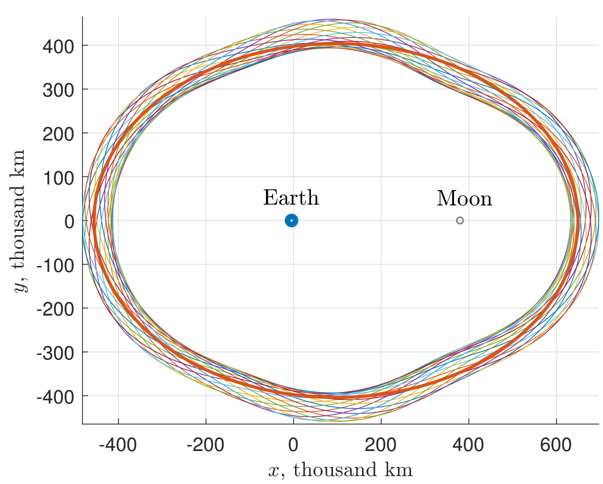

Figure 2. Earth-Moon RoP boundaries for different Sun phase angles and the orange elliptical boundary of the mean-square averaged RoP.

curves, while the averaged elliptic boundary is illustrated by orange line. In the dimensionless system of units specified in Eq. (1), the elliptic boundary satisfies the equation

$$\frac{(x+c)^2}{a^2} + \frac{y^2}{b^2} = 1, \tag{4}$$

where $a = 1.44$, $b = 1.05$, $c = -0.25$. Further, the region of prevalence is understood as the area with the boundary given by Eq. (4).

DESIGN OF PLANAR WSB TRANSFERS

In this paper, planar WSB trajectories are constructed in two stages. At the first stage, a ballistic lunar trajectory is divided into the three legs: the arriving and departing, lying inside the RoP and calculated in the planar Earth-Moon circular restricted three-body problem, and the exterior leg, designed in the Earth-Moon-Sun planar BR4BP. To obtain a whole trajectory, it is enough to patch the segments on the boundary of the RoP. As will be shown below, upon elegantly parametrizing the departing and arriving legs, the process of designing such a planar WSB trajectory is reduced to solving a nonlinear equation. At the second stage, the trajectories obtained at the first stage are adapted to the planar BR4BP by the multiple shooting technique.

Earth Collision Trajectories

To avoid dependence on a specific near-Earth orbit where a trans-lunar injection impulse (TLI) is applied, collision trajectories that pass through the center of the Earth can be used at the preliminary stages of WSB trajectory design.[24] Subsequently, such a trajectory can be numerically adapted so that it starts on a desired near-Earth orbit. Furthermore, after the Levi-Chivita regularization[24] $(u, v) \leftrightarrow (x, y)$ and transition to a new independent variable — fictitious time τ, the spacecraft's velocity (u', v') at the center of the Earth for a given J_{EM} can be parametrized with one angle $\varphi \in [0; \pi]$:

$$u' = \sqrt{\frac{1-\mu}{2}} \cos\varphi,\ v' = \sqrt{\frac{1-\mu}{2}} \sin\varphi,$$

where $u' = du/d\tau$, $v' = dv/d\tau$. The angle φ varies within such limits because between the planes (u, v) and (x, y) is a one-to-two correspondence. Thus, any collision trajectory depends on only two parameters: an ejection angle φ and a Jacobi constant J_{EM}.

Targeting of arriving legs with specified parameters

What concerns the arriving leg, it is also possible to avoid the strict dependence on a specific near-Moon final orbit. As it is well known, for a planar trajectory to be transit (i.e., passing inside the lunar Hill sphere), it should belong to the interior of the stable manifold tube of the L_2 planar Lyapunov orbit with the corresponding Jacobi integral level.

In the $(x,\ \dot{x})$ plane, a bunch of the manifold trajectories, when propagated backward in time, forms a closed curve on the boundary of the RoP, the L_2 lunar gateway (orange line in Figure 3). We denote a set of inner points of the gateway by P. For any $(x_P, \dot{x}_P) \in P$, the corresponding coordinate y_P may be found from the condition of belonging to the boundary of the RoP, while $\dot{y}_P$ is specified by the energy relation $J(x_P, y_P, \dot{x}_P, \dot{y}_P) = J_{EM}$. The propagation of the initial condition $\mathbf{x}_P = [x_P, y_P, \dot{x}_P, \dot{y}_P]$ in the CR3BP will give a trajectory passing inside the Hill sphere of the Moon. Each specific $\mathbf{x}_P$ corresponds to an arriving trajectory with a certain value of the perilune distance r_p and the argument of perilune ω_p, which allows targeting a desired trajectory.

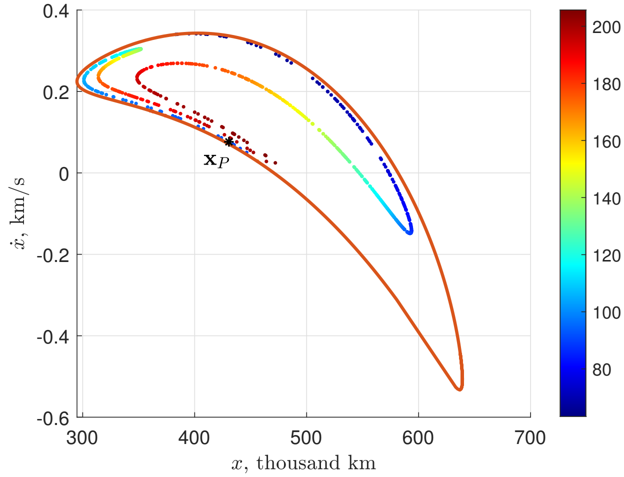

Figure 3. L_2 lunar gateway for $J_{EM} = 3.06$ (orange closed curve) and the perilune altitude contour line corresponding to the perilune altitude value 1403 km. The color of contour line points indicates the argument of perilune (the angle between the Earth-Moon line and the direction to the perilune of a transit trajectory). A certain point of the gateway is marked by $\mathbf{x}_P$.

Figure 3 shows the gradient-colored contour line $r_p = 3141$ km on the L_2 gateway corresponding to $J_{EM} = 3.06$. Such values of the Jacobi integral and perilune distance coincide with the values for the near-rectilinear resonant halo orbit 9:2. The color of the contour line points indicates the ω_p value of the approaching trajectory. Consequently, to obtain the arriving leg with specified r_p and ω_p values, the corresponding point of P should be targeted when the exterior leg of a WSB trajectory is designed. However, not all points are equally convenient for WSB trajectories to pass through.

It is worth noting that the L_2 lunar gateway collapses to a point when $J_{EM} \approx 3.18$, therefore getting the entire WSB trajectory to lunar orbits with $J_{EM} > 3.18$ may become problematic, and such transfers require additional LOI impulse. For almost Keplerian orbits around the Moon, $J_{EM} \approx 3 + W_z - 2E$, where W_z is the z-component of the orbital momentum of a spacecraft, and E is the Keplerian energy in the spacecraft-Moon two-body system. In the planar case, this expression can be rewritten in terms of the distance to the perilune r_p and perilune velocity v_p as $J_{EM} = 3 + r_p v_p - v_p^2 + 2\mu/r_p$. Thus, the required lunar orbit insertion (LOI) impulse at the perilune of the arriving trajectory can be estimated as a solution of the quadratic equation $\Delta J_{EM} \approx \Delta v^2 + 2v\Delta v$. However, in order to avoid additional problems arising when J_{EM} is too close to the gateway closing threshold, it is preferable to target points of the gateways with the values of the Jacobi integral J_{EM} in the range $3.05 \ldots 3.15$.

Designing planar WSB transfers

Let us briefly describe the methodology by which the planar WSB trajectories are calculated. At the first stage, we obtain a whole trajectory by patching its legs on the boundary of the RoP. For a given point $\mathbf{x}_P = [x_P, y_P, \dot{x}_P, \dot{y}_P]$ of the gateway P with a certain value of the Jacobi integral (see Fig. 3), the phase of the Sun θ_P specifies a certain exterior leg outside the RoP when propagating $\mathbf{x}_P$ in the BR4BP backward in time. If, for some value of θ_P, the corresponding exterior leg intersect the boundary of the RoP at some point $\mathbf{x}_P^B = \mathbf{x}_P^B(\mathbf{x}_P, \theta_P)$, we try to retrieve an Earth collision trajectory of the required value of the Jacobi integral $J_{EM}^B = J_{EM}(\mathbf{x}_P^B)$ which provides a zero residue with $\mathbf{x}_P^B$ by varying the departure trajectory angle φ. Let $\mathbf{x}_E^B = \mathbf{x}_E^B(J_{EM}^B, \varphi)$ be used to denote the spacecraft state vector obtained by the intersection of the collision trajectory corresponding to J_{EM}^B and φ with the RoP. Thus, for a given $\mathbf{x}_P$ and some θ_P, the WSB trajectory design is reduced to solving the following nonlinear equation:

$$F(\varphi) = |\mathbf{x}_E^B(\varphi) - \mathbf{x}_P^B| = 0. \tag{5}$$

This equation can be easily solved numerically.[24] Different values of θ_P determine different solutions of the equation. These solutions represent WSB trajectories passing through a fixed point $\mathbf{x}_P$, and $\mathbf{x}_P$ defines an arriving leg with certain values of r_p and ω_p. If we iterate all points $\mathbf{x}_P$ of the gateway P with some value of the Jacobi integral, then a set of planar WSB trajectories corresponding to different values of r_p and ω_p will be obtained. To get arriving trajectories with other values of the Jacobi integral, it is necessary to work with the relevant gateways.

Trajectories calculated at the first stage can then be easily adapted to the trajectories in the planar BR4BP departing from a specific near-Earth parking orbit by the multiple shooting method (for details of the shooting procedure see the Appendix section). This is the second stage of WSB trajectory construction. It is worth noting that in order to get a larger number of WSB trajectories, a small discrepancy (1e-4 in this work) can be allowed in Eq. (5). This discrepancy will then be smoothed by the multiple shooting procedure. The above-described two-stage algorithm was readily implemented using MATLAB's `fsolve` and `fmincon` functions. The convergence of the numerical procedures was rapid and straightforward. As a result, a database of planar WSB transfers to different orbits around the Moon was obtained in the BR4BP model. Trajectories from this database represent a good initial guess for the subsequent adaptation to the real three-dimensional WSB transfers.[24] It is also worth noting that the database contains, among others, transfers with lunar flybys.

Further, we consider planar WSB transfers from the circular near-Earth parking orbit with an altitude of 200 km to the near-Moon orbits with $J_{EM} = 3.06$ and the perilune altitude value of 1403 km. For the analysis of planar WSB trajectories, it is convenient to introduce a new rotating reference frame $Cx'y'$ with the x-axis directed along the line connecting the Sun and the barycenter of the Earth-Moon system (see Figure 4). For all WSB trajectories, its apogees are located in the second or fourth quadrant of the $Cx'y'$ system. Under this condition, the gravitational perturbation from the Sun provides $\Delta J_{EM} > 0$ along along the exterior leg, which is a necessary condition for subsequent ballistic capture. This well-known result of the WSB theory, previously numerically discovered by many researchers, has been analytically explained in the framework of the BR4BP model.[24] Figure 5 shows an example of WSB trajectory obtained at the first stage and the corresponding trajectory after the multiple shooting procedure in the $Cx'y'$ reference frame. The departure and arriving legs of the initial-guess trajectory are drawn in light blue and green, respectively. The exterior leg has a purple hue. The yellow curve represents the circular orbit of the Moon. The resulting WSB trajectory in the BR4BP model is represented in blue. The arriving near-Moon orbit for both trajectories corresponds to the point $\mathbf{x}_P$ indicated by black '$*$' in Figure 3. The time of flight is equal to 115 days. For the Earth collision orbit, $C_3 = -1.52$ km^2/s^2 and $\varphi = 34°$. The initial phase of the Sun θ_0 is 56°. For the adapted trajectory, the TLI impulse $\Delta V_{TLI} = 3.173$ km/s, with almost zero correction and insertion impulses ($\Delta V_{TCM} + \Delta V_{LOI} = 4.22$ m/s).

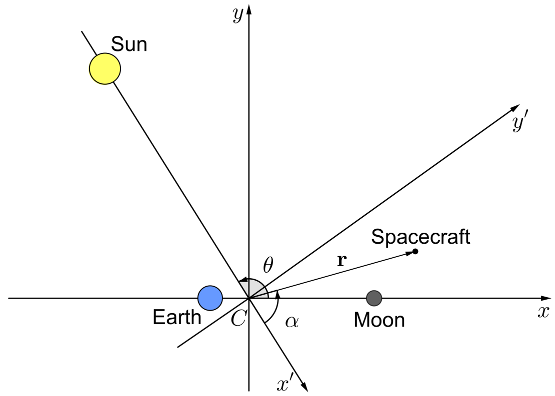

Figure 4. The Earth-Moon rotating reference frame Cxy and the Sun-barycenter rotating reference frame $Cx'y'$. In the Sun-barycenter coordinate system, the spacecraft radius vector is described by the polar angle α.

Planar WSB Trajectories with a Lunar Flyby

The lunar-gravity-assisted WSB transfers are grouped by the exit point from the Earth-Moon RoP. It appeared that it is convenient to display their characteristics on the boundary of RoP on the (y, γ) plane, where γ is the angle between the spacecraft's radius vector and velocity. Figure 6 describes the set of 453 trajectories including an intermediate lunar flyby after the departure from the circular near-Earth parking orbit with an altitude of 200 km and arriving to the near-Moon orbits with $J_{EM} = 3.06$ and the perilune altitude of 1403 km. The figure shows that such transfers are grouped in a rather narrow range from -320 to -240 thousand km in y and from $55°$ to $58.5°$ in γ.

As for the characteristics of the presented lunar-gravity-assisted trajectories, the launch energy C_3 varies from -1.2 to -2 km^2/s^2 (see Figure 6, a), which corresponds to the TLI impulses ΔV_{TLI} applied in the 200 km circular near-Earth orbit in the range from 3.15 to 3.19 km/s (Figure 6, b). The time of flight for the obtained trajectories varies from 80 to 220 days (see Figure 6, c). In addition, Figure 6, d confirms the fulfillment of the property of the second/fourth quadrant of the $Cx'y'$ reference frame. The RoP exit points are grouped near two values of the angle $\alpha \approx \approx 130°$ (the second quadrant) and $\alpha \approx 310°$ (the fourth quadrant). Using such colored plots, it is possible to display many other properties of the trajectories. Subsequently, when designing lunar-gravity-assisted transfers with desired characteristics, the corresponding points of the plane (y, γ) are convenient to be targeted.

TARGETING WSB TRAJECTORIES WITH A LUNAR FLYBY

Targeting Algorithm

It would be desirable to analytically target a certain WSB trajectory with a lunar flyby. It means that knowing exiting parameters on the boundary of the RoP, we need to determine the parameters of a TLI impulse that results in the desired trajectory with a gravity-assist maneuver near the Moon. To tackle this problem, we use the patched conic approximation. Further, we imply that all the parameters are expressed in the dimensionless system of units introduced by Eq. (1).

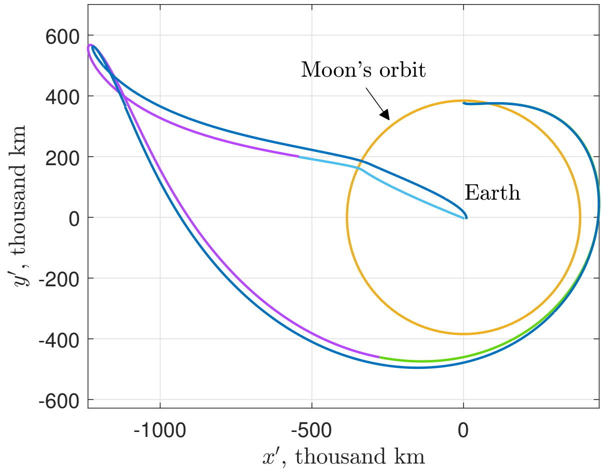

Figure 5. An initial-guess planar WSB trajectory consisting of the departing (light blue), exterior (purple) and arriving (green) legs, and the corresponding adapted trajectory departing from the 200 km near-Earth parking orbit in the BR4BP model. The time of flight is 115 days. The TLI impulse $\Delta \mathbf{V_{TLI}} = 3.173$ km/s, the sum of trajectory correction and lunar orbit insertion impulses $\Delta \mathbf{V_{TCM}} + \Delta \mathbf{V_{LOI}} = 4.22$ m/s.

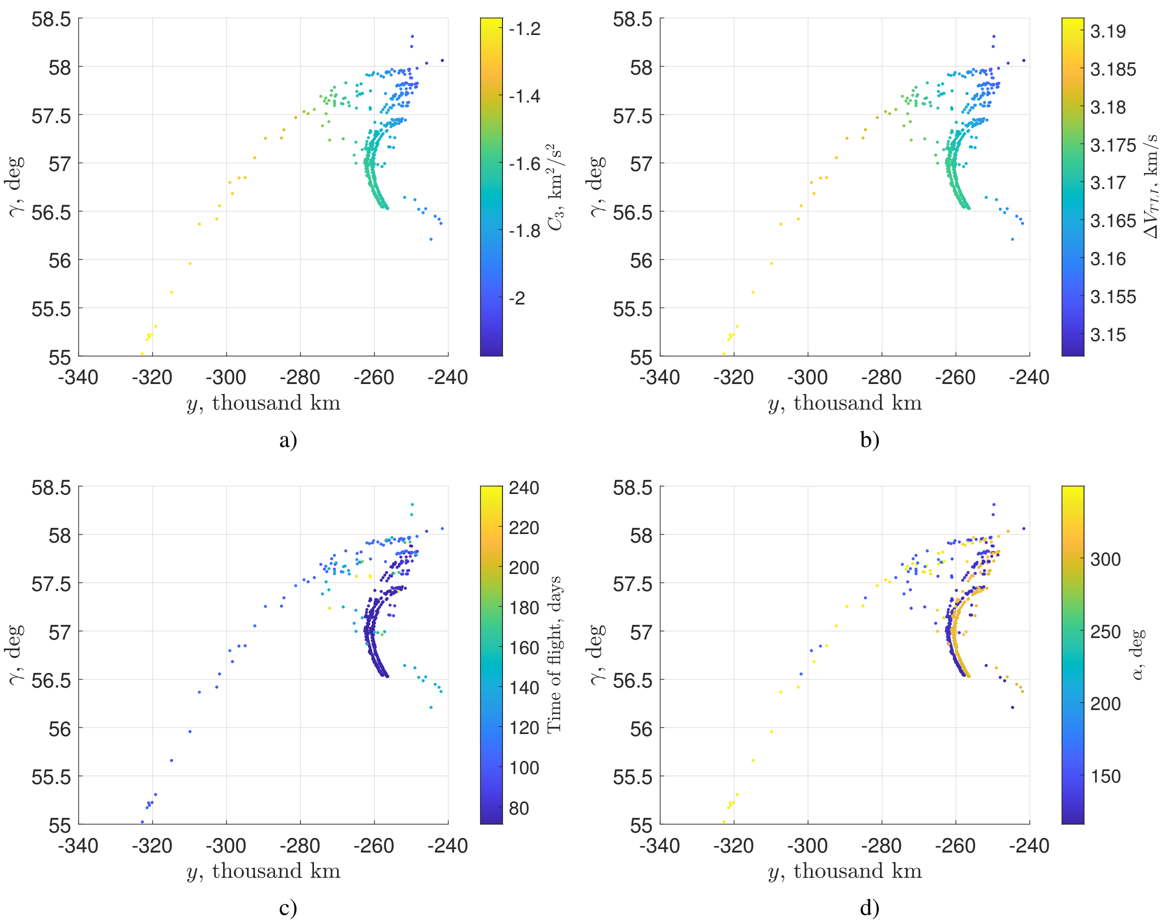

Figure 6. Lunar-gravity-assisted planar WSB transfers parameters when crossing the boundary of the Earth-Moon RoP. The angle between the spacecraft's radius vector and velocity counted clockwise is denoted by γ. The color bars describe different characteristics of WSB trajectories. The α angles are given at the moment of crossing the RoP boundary and grouped around two values in the second and fourth quadrant.

Let us suppose that a spacecraft is orbiting the Earth in a circular orbit with a given altitude, and at some time moment t_0 a departure TLI impulse $\Delta \mathbf{V}_{TLI}$ directed along the spacecraft's velocity is applied. Characteristics of the TLI impulse fully determine the post-impulse geocentric orbit parameters. The TLI impulse epoch t_0 relates to the spacecraft's argument of perigee ψ_π with respect to some axis of the geocentric inertial frame (see Figure 7), while the magnitude of the impulse ΔV_{TLI} determines the focal parameter p and the eccentricity e. The position of the Moon is assumed to be defined by angle ϕ called the lunar phase; at the moment when the impulse is applied, the lunar phase is denoted as ϕ_0. The spacecraft's true anomaly is denoted by ν.

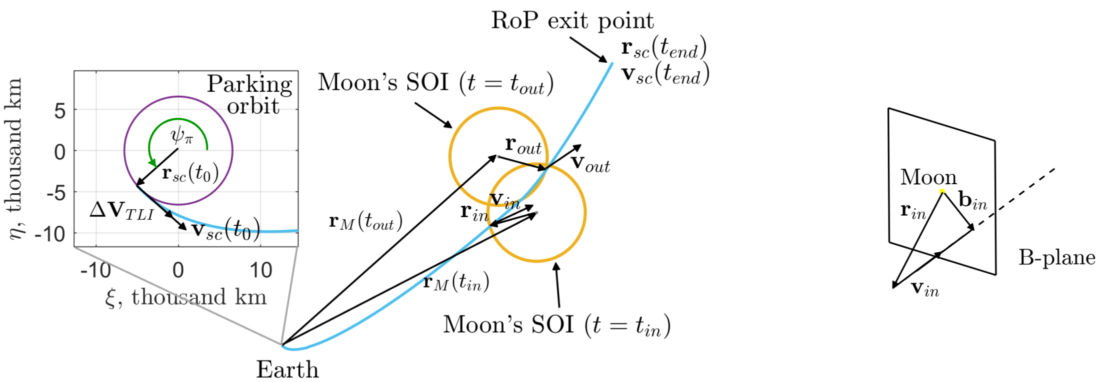

Figure 7. Interior leg of WSB trajectory in the Earth-centered inertial reference frame. B-plane is exploited to calculate the flyby characteristics.

First, having all the parameters of the spacecraft's orbit after the TLI impulse, we can find the moment t_{in} when the spacecraft enters the lunar SOI. The condition of entering the SOI is

$$|\mathbf{r}_{sc} - \mathbf{r}_M|^2 = r_{SOI}^2, \tag{6}$$

where $\mathbf{r}_{sc}$ is the radius vector from the Earth to the spacecraft, $\mathbf{r}_M$ is the radius vector from the Earth to the Moon. These vectors can be written in terms of the parameters of the spacecraft's orbit and the angle ϕ:

$$\begin{gathered}\mathbf{r}_{sc} = \frac{p}{1 + e\ \cos\nu}[\cos(\nu + \psi_\pi), \sin(\nu + \psi_\pi)], \\ \mathbf{r}_M = [\cos\phi, \sin\phi].\end{gathered} \tag{7}$$

We assume that we know the lunar phase at t_{in} and denote it as ϕ_{in}. We also denote the true anomaly at this moment as ν_{in}. Then we substitute Eq. (7) into the entering condition given by Eq. (6). Upon defining $\psi = \psi_\pi - \phi_{in}$ and $\varkappa = 1 + e\cos\nu_{in}$ and assuming $\nu_{in} \in [0;\ \pi]$, (i.e., $\sin\nu_{in} = \sqrt{1 - \cos^2\nu_{in}}$), we obtain

$$\varkappa^2\delta_2 - 2\varkappa\frac{\delta_1}{e}(\varkappa - 1)\cos\psi + 1 = -2\varkappa\delta_1\sqrt{1 - \frac{(\varkappa - 1)^2}{e^2}}\sin\psi, \tag{8}$$

where

$$\begin{gathered}\delta_1 = \frac{1}{p}, \\ \delta_2 = \frac{1 - r_{SOI}^2}{p^2}.\end{gathered}$$

When squared, Eq. (8) is transformed into

$$a_4\varkappa^4 + a_3\varkappa^3 + a_2\varkappa^2 + a_1\varkappa + a_0 = 0, \tag{9}$$

where

$$\begin{aligned}
a_4 &= \delta_2^2 - \frac{4\delta_1\delta_2\cos\psi}{e} + \frac{4\delta_1^2}{e^2},\\
a_3 &= -\frac{8\delta_1^2}{e^2} + \frac{4\delta_1\delta_2\cos\psi}{e},\\
a_2 &= 4\delta_1^2\left(\frac{1}{e^2} - \sin^2\psi\right) - \frac{4\delta_1\cos\psi}{e} + 2\delta_2,\\
a_1 &= \frac{4\delta_1\cos\psi}{e},\\
a_0 &= 1.
\end{aligned}$$

Equation (9) can be solved analytically using Ferrari's method, so we assume that up to four solutions are known. Then these solutions must be checked for satisfying Eq. (8), because Eq. (9) allows solutions with $\nu_{in} \in [\pi;\ 2\pi]$. Among the remaining solutions (if they exist), the least ν_{in} is chosen. This procedure provides us with the solution $\nu_{in}(\phi_{in})$ of Eq. (6).

Now it is time to relate ϕ_{in} with ϕ_0. The epoch t_{in} when the spacecraft enters the SOI can be calculated from Kepler's equation

$$\begin{aligned}
t_{in} - t_0 &= \sqrt{\frac{p^3}{\mu_E(1-e^2)^3}}\left(E_{in} - e\sin E_{in}\right),\\
E_{in} &= 2\arctan\sqrt{\frac{1-e}{1+e}}\tan\frac{\nu_{in}}{2},
\end{aligned} \tag{10}$$

where μ_E is the Earth's gravitational parameter, $\mu_E = 398600.4356$ km^3/s^2. Knowing the time of the flight, we can easily find ϕ_{in}:

$$\phi_{in} = \phi_0 + (t_{in} - t_0). \tag{11}$$

Equations (8), (9), (10), (11) together form a nonlinear equation that can be solved iteratively (using the simple-iteration method) for ϕ_{in} from which ν_{in} can be calculated with Eq. (9). Thus we obtain the true anomaly and the lunar phase at the epoch of entering the SOI.

The next step is the analysis of the spacecraft's lunar flyby. It can be performed by utilizing the B-plane.[20] From ν_{in} and ϕ_{in}, we can obtain $\mathbf{r}_{sc}$ and $\mathbf{r}_M$ using Eq. (7), while the spacecraft's and Moon's velocities $\mathbf{v}_{sc}$, $\mathbf{v}_M$ are calculated by the formulas

$$\begin{aligned}
\mathbf{v}_{sc} &= \sqrt{\frac{\mu_E}{p}}[-\sin(\nu+\psi_\pi) - e\sin\psi_\pi, \cos(\nu+\psi_\pi) + e\cos\psi_\pi],\\
\mathbf{v}_M &= [-\sin\phi, \cos\phi].
\end{aligned} \tag{12}$$

Having these vectors, we calculate the spacecraft's position and velocity relative to the Moon at the epoch of entering the SOI

$$\begin{aligned}
\mathbf{r}_{in} &= \mathbf{r}_{sc}\left(\nu_{in}\right) - \mathbf{r}_M\left(\phi_{in}\right),\\
\mathbf{v}_{in} &= \mathbf{v}_{sc}\left(\nu_{in}\right) - \mathbf{v}_M\left(\phi_{in}\right),
\end{aligned}$$

and the B-vector (see Figure 7)

$$\mathbf{b}_{in} = \mathbf{r}_{in} - \frac{\mathbf{v}_{in} \cdot \mathbf{r}_{in}}{|\mathbf{v}_{in}|^2}\mathbf{v}_{in}.$$

Using $\mathbf{v}_{in}$ and $\mathbf{b}_{in}$, it is possible to retrieve the parameters of the spacecraft's hyperbolic celenocentric orbit

$$C_h = |\mathbf{b}_{in}|\,|\mathbf{v}_{in}|\,,$$
$$h_h = |\mathbf{v}_{in}|^2 - \frac{2\mu_M}{r_{SOI}},$$
$$p_h = \frac{C_h^2}{\mu_M},$$
$$e_h = \sqrt{1 + h_h \frac{C_h^2}{\mu_M^2}},$$
$$r_{\pi,h} = \frac{p_h}{1 + e_h},$$

where μ_M is the gravitational parameter of the Moon, $\mu_M = 4902.8001$ km^3/s^2. The selenocentric distance and speed when the spacecraft leaves the SOI are bound to be equal to respective values at the moment the spacecraft enters the SOI:

$$|\mathbf{v}_{out}| = |\mathbf{v}_{in}|\,,$$
$$|\mathbf{b}_{out}| = |\mathbf{b}_{in}|\,,$$
$$|\mathbf{r}_{out}| = |\mathbf{r}_{in}| = r_{SOI}.$$

Thus, to determine the spacecraft's geocentric orbit after the flyby, we only have to know how $\mathbf{v}_{out}$ and $\mathbf{b}_{out}$ are directed and how much time it takes the spacecraft to leave the SOI. To determine the vectors directions, we calculate the bending angle[20] taking into account that the spacecraft's lunar flyby actually starts and ends at the SOI boundary, not at the infinity:

$$\delta = \delta_\infty - 2\Delta,$$

where

$$\delta_\infty = 2\arcsin \frac{1}{1 + r_{\pi,h}\left(\dfrac{|\mathbf{v}_{in}|^2}{\mu_M} - \dfrac{2}{r_{SOI}}\right)},$$

$$\Delta = -\arccos\frac{1}{e_h} + \arccos\left(\frac{1}{e_h}\sqrt{\frac{e_h^2 - \left(1 - \dfrac{p_h}{r_{SOI}}\right)^2}{e_h^2 + 2\,\dfrac{p_h}{r_{SOI}} - 1}}\right).$$

Having calculated δ, we can find $\mathbf{v}_{out}$, $\mathbf{b}_{out}$ and $\mathbf{r}_{out}$:

$$\mathbf{v}_{out} = \left(\cos\delta\frac{\mathbf{v}_{in}}{|\mathbf{v}_{in}|} - \sin\delta\frac{\mathbf{b}_{in}}{|\mathbf{b}_{in}|}\right)|\mathbf{v}_{in}|\,,$$
$$\mathbf{b}_{out} = \left(\cos\delta\frac{\mathbf{b}_{in}}{|\mathbf{b}_{in}|} + \sin\delta\frac{\mathbf{v}_{in}}{|\mathbf{v}_{in}|}\right)|\mathbf{b}_{in}|\,,$$
$$\mathbf{r}_{out} = \mathbf{b}_{out} + \frac{\mathbf{v}_{out}}{|\mathbf{v}_{in}|}\sqrt{r_{SOI}^2 - |\mathbf{b}_{in}|^2}.$$

The time the spacecraft spends in the SOI is obtained using Kepler's equation

$$t_h = 2\sqrt{\frac{p_h^3}{\mu_M\left(e_h^2-1\right)}}\left(e\sinh H' - H'\right),$$
$$H' = 2\,\mathrm{arctanh}\left(\sqrt{\frac{e_h-1}{e_h+1}}\tan\frac{\nu'}{2}\right),$$
$$\nu' = \arccos\left(\frac{1}{e_h}\left(\frac{p_h}{r_{SOI}}-1\right)\right).$$

Hence, we are able to determine the lunar phase at the moment the spacecraft leaves the SOI

$$\phi_{out} = \phi_{in} + t_h,$$

$t_{out} = t_{in} + t_h$, and the geocentric orbit parameters after the flyby p_{out}, e_{out}, $\psi_{\pi,out}$ are calculated as follows:[26]

$$\mathbf{r}_{sc,out} = \mathbf{r}_{out} + \mathbf{r}_M(\phi_{out}),$$
$$\mathbf{v}_{sc,out} = \mathbf{v}_{out} + \mathbf{v}_M(\phi_{out}).$$

The last step is the determination of the spacecraft's exiting point on the RoP boundary, which is defined by Eq. (4) in the rotating frame. Since in this chapter we use the Earth-centered inertial frame, we have to rewrite the RoP boundary equation in the following form

$$\frac{(x-x_c)^2}{a^2} + \frac{y^2}{b^2} = 1, \tag{13}$$

where $(x,\, y)$ are coordinates in the Earth-centered rotating frame and

$$x_c = -c + \mu = 0.25 + \mu.$$

Let us suppose that we know the lunar phase at the moment t_{end} when the spacecraft reaches the RoP boundary and denote it as ϕ_{end}. For the spacecraft's true anomaly on the RoP boundary ν_{end}, we further denote $\cos\nu_{end}$ as ρ and assume $\nu_{end} \in [0;\, \pi]$, (i.e., $\sin\nu_{end} = \sqrt{1-\cos^2\nu_{end}}$). Substituting spacecraft's coordinates obtained from Eq. (7) into Eq. (13) yields

$$\frac{\left(\alpha_1\rho + \alpha_2\sqrt{1-\rho^2} + \alpha_0\left(1+e_{out}\rho\right)\right)^2}{a^2} + \frac{\left(-\alpha_2\rho + \alpha_1\sqrt{1-\rho^2}\right)^2}{b^2} = \frac{\left(1+e_{out}\rho\right)^2}{p_{out}^2}, \tag{14}$$

where

$$\alpha_0 = -\frac{x_c}{p_{out}},$$
$$\alpha_1 = \cos\left(\psi_{\pi,out} - \phi_{end}\right),$$
$$\alpha_2 = \sin\left(-\psi_{\pi,out} + \phi_{end}\right).$$

Equation (14) can be rewritten as

$$\beta_2\rho^2 + \beta_1\rho + \beta_0 = -\sqrt{1-\rho^2}\left(\beta_1'\rho + \beta_0'\right), \tag{15}$$

where

$$\beta_0 = \frac{\alpha_0^2 + \alpha_2^2}{a^2} + \frac{\alpha_1^2}{b^2} - \frac{1}{p_{out}^2},$$
$$\beta_0' = 2\frac{\alpha_0\alpha_2}{a^2},$$
$$\beta_1 = 2\frac{\alpha_0\left(\alpha_1 + e_{out}\alpha_0\right)}{a^2} - 2\frac{e_{out}}{p_{out}^2},$$
$$\beta_1' = 2\alpha_2\left(\frac{\alpha_1 + e_{out}\alpha_0}{a^2} - \frac{\alpha_1}{b^2}\right),$$
$$\beta_2 = \frac{\left(\alpha_1 + e_{out}\alpha_0\right)^2 - \alpha_2^2}{a^2} + \frac{\alpha_2^2 - \alpha_1^2}{b^2} - \frac{e_{out}^2}{p_{out}^2}.$$

Squaring Eq. (15), we get

$$\gamma_4\rho^4 + \gamma_3\rho^3 + \gamma_2\rho^2 + \gamma_1\rho + \gamma_0 = 0 \tag{16}$$

where

$$\gamma_4 = \beta_2^2 + \beta'^2_1,$$
$$\gamma_3 = 2\left(\beta_1\beta_2 + \beta_0'\beta_1'\right),$$
$$\gamma_2 = \beta'^2_0 + \beta_1^2 - \beta'^2_1 + 2\beta_0\beta_2,$$
$$\gamma_1 = 2\left(\beta_0\beta_1 - \beta_0'\beta_1'\right),$$
$$\gamma_0 = \beta_0^2 - \beta'^2_0.$$

Similarly to Eq. (9), we have a fourth-order equation that can be solved using Ferrari's method. It provides up to four solutions, and each one should be checked for satisfying Eq. (15) because we need only the solutions related to the positive $\sin\nu_{end}$, whereas Eq. (16) allows negative ones. After that, we obtain from zero to two solutions for $\cos\nu_{end}$ which we convert into values of ν_{end} and in case of two solutions, we choose the one that is the closest to the ν_{out}.

Searching for ν_{end}, we again assumed that we know ϕ_{end}, but in fact they are mutually dependent. The time the spacecraft flies to the RoP boundary after leaving the SOI can be calculated by means of Kepler's equation

$$\begin{gathered} t_{out-end} = \sqrt{\frac{p_{out}^3}{\mu_E(1-e_{out}^2)^3}}\left(E_{end} - E_{out} - e\left(\sin E_{end} - \sin E_{out}\right)\right), \\ E_{out} = 2\arctan\sqrt{\frac{1-e_{out}}{1+e_{out}}}\tan\frac{\nu_{out}}{2}, \\ E_{end} = 2\arctan\sqrt{\frac{1-e_{out}}{1+e_{out}}}\tan\frac{\nu_{end}}{2}, \end{gathered} \tag{17}$$

so ϕ_{end} is expressed as

$$\phi_{end} = \phi_{out} + t_{out-end}. \tag{18}$$

Equations (15), (16), (17), (18) together can be interpreted as nonlinear equation on ϕ_{end} that can be solved using iterative methods (e.g., the simple-iteration method). When ϕ_{end} and ν_{end} are found, one can straightforwardly calculate $\mathbf{r}_{sc}$ and $\mathbf{v}_{sc}$ on the RoP boundary by Eq. (7) and Eq. (12). Based on these vectors and the lunar phase, any other characteristics can be retrieve.

Following the procedure described in this chapter, one can calculate the parameters of exiting the RoP based on the parameters of the TLI impulse or, vice versa, can get the departure parameters for a given point of the RoP boundary. The procedure does not require any numerical integration, though needs a couple of nonlinear equations need to be solved numerically.

To determine the departure parameters for a given RoP exit point, an inverse problem should be solved. It can be done using the same analytical tools. However, in our case, it is enough to go through a set of the spacecraft's departure parameters ΔV_{TLI} and ψ_π in order to generate a grid of contour lines in the (y, γ) plane that can be used for visual assessment of the departure parameters for the point desired.

Figure 8 shows the contour lines of the magnitude of the TLI impulse ΔV_{TLI} (a) and the spacecraft's initial argument of perigee ψ_π (b) of the 200 km circular near-Earth parking orbit for the pairs (y, γ) on the boundary of the RoP. These contour lines were calculated analytically from the patched conic approximation by varying ΔV_{TLI} from 3.15 km/s to 3.19 km/s and ψ_π from 215° to 226°. The colored points correspond to the lunar-gravity-assisted WSB trajectories previously obtained in the BR4BP model (see Figure 6, b). As seen from Figure 8, a, the analytical results quite accurately conform to the numerical results obtained in the BR4BP model. Since the pair $(\Delta V_{TLI}, \psi_\pi)$ uniquely defines a specific trajectory with a lunar flyby in the patched conic approximation model, the isolines in Figure 8, a-b, give an estimate of the required departure parameters that ensure the pairs (y, γ) on the boundary of the RoP that correspond to WSB transfers. In other words, targeting a certain lunar-gravity-assisted WSB transfer is carried out by defining the corresponding ΔV_{TLI} and ψ_π. Such analytical estimates make it possible to avoid any numerical optimization at the preliminary stages of mission design.

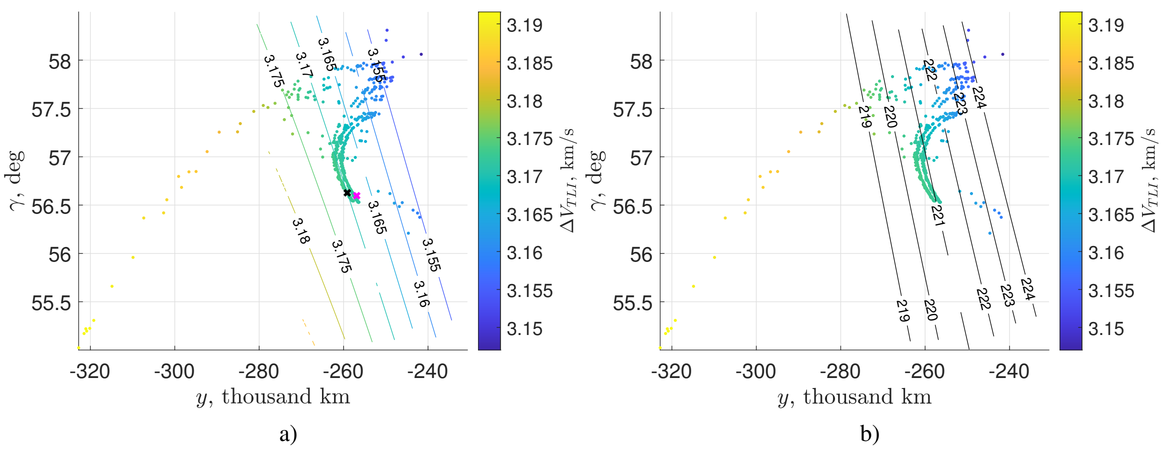

Figure 8. Contour lines of the magnitude of the TLI impulse $\mathbf{\Delta V_{TLI}}$ (a) and the spacecraft's initial argument of perigee ψ_π (b) for the case of the 200 km circular parking orbit analytically calculated from the patched conics model, WSB trajectories characteristics on the RoP boundary obtained in the BR4BP model are shown by colored dots.

It should also not be forgotten that in the BR4BP model, the exterior leg of the trajectory strongly depends on the phase of the Sun at the epoch of crossing the boundary of the RoP. Since within the framework of the patched conic approximation model the values of ΔV_{TLI} and ψ_π at the epoch t_0 uniquely determine the time of flight T from the parking orbit to the RoP boundary, a desired phase θ_0 at the epoch t_0 can be simply calculated from a given phase of the Sun on the boundary of the RoP using Eq. (3). So, in more complex models of motion, the epoch t_0 can be selected in accordance with θ_0.

Targeting Algorithm Validation

The obtained analytical estimates are quite accurate when switching to the planar BR4BP model. If we take the initial parameters ΔV_{TLI} and ψ_π corresponding to a certain point (y_1, γ_1) from the patched conic approximation model, determine the required phase of the Sun θ_0, and based on these values, propagate the spacecraft's equation of motion in the BR4BP model until the intersection with the RoP, the resulting point on the boundary of the RoP (y_2, γ_2) will be close enough to (y_1, γ_1). As an example, in Figure 8, we mark by the black cross 'x' a certain point (y_1, γ_1) and by the rose 'x' the respective point (y_2, γ_2).

To get exactly the point (y_1, γ_1) in the BR4BP model, the initial parameters ΔV_{TLI} and ψ_π can be slightly adjusted by the multiple shooting procedure (the details of the procedure can be found in Appendix). For the points considered above, as a result of the multiple shooting adaptation, the initial argument of perigee ψ_π has been changed by $0.8°$, the TLI impulse ΔV_{TLI} has been increased by 3.6 m/s, and the additional correction impulse of 9.9 m/s on the boundary of the RoP was introduced. Figure 9 shows the trajectory integrated in the BR4BP model with initial parameters from the patched conic approximation (red-green dashed line) and the corresponding adjusted trajectory after applying the multiple shooting algorithm (blue, almost covering the first trajectory) in the Earth-Moon rotating reference frame. The black crosses are related to the trajectory in the patched conic approximation model and correspond to the nodes of the multiple shooting method. For different points of the plane (y, γ), the multiple shooting method converges straightforwardly and rapidly, providing small corrections in the initial parameters. Therefore, the analytical solution represents a good initial guess when targeting lunar-gravity-assisted WSB transfers in the planar BR4BP model. The resulting planar transfers including a lunar flyby can then be used as an initial guess for the subsequent adaptation to the realistic three-dimentional WSB transfers from a specific near-Earth parking orbit with nonzero inclination to a desired lunar orbit.[24]

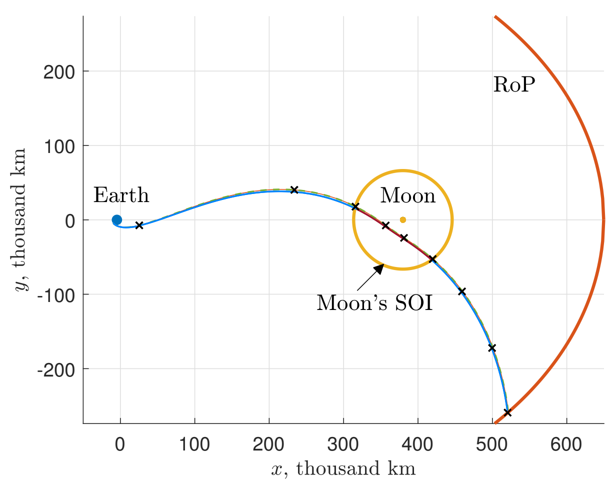

Figure 9. An example of a trajectory integrated in the BR4BP with initial parameters from the patched conic approximation (red-green dashed line) and the corresponding adjusted trajectory after applying the multiple shooting algorithm (blue) in the Earth-Moon rotating reference frame.

CONCLUSION

The paper presented a set of analytical formulas that give a good estimate of the departure parameters (i.e., the magnitude of the TLI impulse and the point of its application) from the near-Earth parking orbit providing a lunar flyby for a desired planar WSB transfer. The characteristics of planar lunar-gravity-assisted WSB trajectories, previously constructed numerically in the BR4BP model, are projected on the boundary of the RoP and targeted. It appeared that it is convenient to display the characteristics on the (y, γ) plane, where γ is the angle between the spacecraft's radius vector and velocity. The lunar-gravity-assisted WSB transfers are grouped by the RoP exit point, which narrows the targeting area. Typical values for a set of transfers from the circular near-Earth parking orbit with an altitude of 200 km to the near-Moon orbits with $J_{EM} = 3.06$ and the perilune altitude value of 1403 km vary in a rather narrow range from -320 to -240 thousand km in y and from $55°$ to $58.5°$ in γ.

Using the obtained formulas for the points of the (y, γ) plane, it is possible to visually assess the corresponding TLI impulses ΔV_{TLI} and angles ψ_π defining the initial position of the spacecraft that provide a lunar-gravity-assisted trajectories ending at the desired points on the RoP boundary within the framework of the patched conic approximation. These estimates are quite accurate when switching to the planar BR4BP model. Nonetheless, the parameters can be refined when adapting the trajectory by the multiple shooting method. For different points of the plane (y, γ) the multiple shooting method convergence turned out to be straightforward and rapid with subtle corrections being introduced.

ACKNOWLEDGMENT

The study is funded by the Russian Science Foundation (RSF), project 19-11-00256.

APPENDIX: MULTIPLE SHOOTING PROCEDURE

Let us consider the adaptation of WSB trajectories obtained in simplified models to the BR4BP model so that it starts at a given circular near-Earth orbit of radius R_c at t_0 and ends at a given point in the phase space X_f at t_f.

First, let us define the optimization variables. It is convenient to set the spacecraft's position and velocity in the initial near-Earth parking orbit using a certain angle related to the center of the Earth. Here we set that the inertial coordinate system associated with the Earth $E\xi\eta$ and the standard rotating reference frame of the Earth-Moon system centered at the Earth Exy coincide at the initial epoch $t = 0$. Let us denote the angle measured from the $E\xi$-axis and defining the spacecraft's position at the epoch t_0 by ψ_π (see Figure 7). Thus, the spacecraft's radius vector and velocity in the inertial reference frame at t_0 are determined as follows:

$$\mathbf{r}_0^{ine} = R_c[\cos\psi_\pi, \sin\psi_\pi],$$
$$\mathbf{v}_0^{ine} = V_c[\cos(\psi_\pi + \pi/2), \sin(\psi_\pi + \pi/2)],$$

where $V_c = \mu_E/R_c$ is the orbital velocity in a circular orbit with radius R_c. After the impulse is applied

$$\mathbf{v}_0^{\prime ine} = \mathbf{v}_0^{ine}(1 + \Delta V_{TLI}/v_0^{ine}),$$

where $v_0^{ine} = |\mathbf{v}_0^{ine}|$, ΔV_{TLI} defines the initial trans lunar injection (TLI) impulse. Thus, in the rotating reference frame Cxy

$$\mathbf{r}'_0 = A\mathbf{r}_0^{ine} + [-\mu, 0],$$
$$\mathbf{v}'_0 = A\mathbf{v}_0^{ine} + \begin{pmatrix} 0 & 1 \\ -1 & 0 \end{pmatrix} \mathbf{r}'_0 - [0, \mu],$$
$$A = \begin{pmatrix} \cos t_0 & \sin t_0 \\ -\sin t_0 & cost_0 \end{pmatrix}.$$

So, the initial phase vector $\mathbf{X}'_0 = [\mathbf{r}'_0, \mathbf{v}'_0]$ is determined by the variable ψ_π. The phase vectors in the subsequent nodes of the multiple shooting method $\mathbf{X}_i = [\mathbf{r}_i, \mathbf{v}_i]$ and the corresponding epochs t_i, $i = \overline{1, N}$ are also considered as the variables. The TLI impulse is determined only by its value ΔV_{TLI}. The final lunar orbit insertion impulse we denote by $\Delta \mathbf{V}_{LOI}$. In addition, we allow a small trajectory correction maneuver (TCM) $\Delta \mathbf{V}_{TCM}$ at the trajectory apogee. Thus, ΔV_{TLI}, $\Delta \mathbf{V}_{LOI}$, $\Delta \mathbf{V}_{TCM}$ are also the variables of the method.

Now let us define the constraints. Let $\mathbf{X}_0^t$ defines the phase vector obtained by integration of the BR4BP equations of motion from initial point $\mathbf{X}'_0$ on $[t_0, t_1]$. Thus, the following expression

$$\mathbf{X}_0^t - \mathbf{X}_1 = 0 \tag{19}$$

represents the first equality constraint. Further, we denote as $\mathbf{X}_i^t$ the phase vector obtained by integration of the BR4BP equations of motion from $\mathbf{X}_i$ on the interval $[t_i, t_{i+1}]$, $i = \overline{1, N-1}$. If the node N_{TCM} corresponds to the node of the TCM-impulse applying, therefore, on $[t_{N_{TCM}}, t_{N_{TCM}+1}]$ the BR4BP equations of motion should be integrated from $\mathbf{X}'_{N_{TCM}} = [\mathbf{r}_{N_{TCM}}, \mathbf{v}_{N_{TCM}} + \Delta \mathbf{V}_{TCM}]$. So, we obtain $N-1$ following equality constraints

$$\mathbf{X}_i^t - \mathbf{X}_{i+1} = 0, \;\; i = \overline{1, N-1}. \tag{20}$$

In addition, two more constraints are met at the last point

$$\begin{gathered} \mathbf{X}'_N - \mathbf{X}_f = 0, \\ t_N - t_f = 0, \end{gathered} \tag{21}$$

where $\mathbf{X}'_N = [\mathbf{r}_N, \mathbf{v}_N + \Delta \mathbf{V}_{LOI}]$.

What concerns the inequality constraints, they are as follows:

$$\begin{gathered} t_0 - t_1 \leq 0, \\ t_i - t_{1+1} \leq 0, \;\; i = \overline{1, N-1}, \\ \Delta V_{TLI} - V_1 \leq 0, \end{gathered} \tag{22}$$

where $V_1 = 3.2$ km/s.

Thus, we have a nonlinear programming problem with the equality constraints (19), (20) and (21), and the inequality constraints (22). As a functional, we consider

$$\Delta V_{TCM}^2 + \Delta V_{LOI}^2 \to \text{min}.$$

REFERENCES

[1] T. Gill, "Lunar Orbital Platform-Gateway," *45th Space Congress Proceedings*, Cape Canaveral, Florida, USA, February 27 – March 1, 2018, 27 p.

[2] C. C. Conley, "Low Energy Transit Orbits in the Restricted Three-Body Problem," *SIAM Journal of Applied Mathematics*, Vol. 16, No. 4, 1968, pp. 732–746.

[3] E. A. Belbruno and J. K. Miller, "Sun-Perturbed Earth-to-Moon Transfers with Ballistic Capture," *Journal of Guidance, Control, and Dynamics*, Vol. 16, No. 4, 1993, pp. 770–775.

[4] E. Bollt and J. Meiss, "Targeting Chaotic Orbits to the Moon through Recurrence," *Physics Letters A*, Vol. 204, No. 5, 1995, pp. 373–378.

[5] W. Koon, M. Lo, J. Marsden, and S. Ross, "Shoot the Moon," *Advances in the Astronautical Sciences*, Vol. 105, 2000, pp. 1017–1030.

[6] V. V. Ivashkin, "On Trajectories of Earth–Moon Flight of a Particle with Its Temporary Capture by the Moon," *Doklady Physics*, Vol. 47, No. 11, 2002, pp. 825–827.

[7] J. Parker and R. Anderson, *Low-Energy Lunar Trajectory Design*. Pasadena, California: John Wiley & Sons, 2014.

[8] J. Parker and G. Born, "Modeling a Low-Energy Ballistic Lunar Transfer Using Dynamical Systems Theory," *Journal of Spacecraft and Rockets*, Vol. 45, No. 6, 2008, pp. 1269–1281.

[9] F. Topputo, E. Belbruno, and M. Gidea, "Resonant Motion, Ballistic Escape, and Their Applications in Astrodynamics," *Advances in Space Research*, Vol. 42, No. 8, 2008, pp. 1318–1329.

[10] F. García and G. Gómez, "A Note on Weak Stability Boundaries," *Celestial Mechanics and Dynamical Astronomy*, Vol. 97, No. 2, 2007, pp. 87–100.

[11] E. Belbruno, M. Gidea, and F. Topputo, "Weak Stability Boundary and Invariant Manifolds," *SIAM Journal of Applied Dynamical Systems*, Vol. 9, No. 3, 2010, pp. 1061–1089.

[12] E. Belbruno and J. Miller, "A Ballistic Lunar Capture Trajectory for the Japanese Spacecraft Hiten," Tech. Rep. IOM 312/90.4-1731-EAB, JPL, California Institute of Technology, 1990.

[13] T. Hoffman, "GRAIL: Gravity Mapping the Moon," *Proceedings of the IEEE Aerospace Conference*, Big Sky, Montana, USA, March 7-14, 2009, pp. 293–300.

[14] F. Topputo, "On Optimal Two-Impulse Earth-Moon Transfers in a Four-Body Model," *Celestial Mechanics and Dynamical Astronomy*, Vol. 117, 2013, pp. 279–313.

[15] N. Parrish, E. Kayser, S. Udupa, J. Parker, B. Cheetham, and D. Davis, "Survey of Ballistic Lunar Transfers to Near Rectilinear Halo Orbit," *Advances in the Astronautical Sciences*, Vol. 171, 2019, pp. 1003–1022.

[16] K. Yagasaki, "Sun-Perturbed Earth-to-Moon Transfers with Low Energy and Moderate Flight Time," *Celestial Mechanics and Dynamical Astronomy*, Vol. 90, No. 3, 2004, pp. 197–212.

[17] G. Lantoine, T. McElrath, and P.Timothy, "Families of Solar-Perturbed Moon-to-Moon Transfers," *Advances in the Astronautical Sciences*, Vol. 152, 2014, pp. 3721–3736.

[18] D. Yárnoz, C. Yam, S. Campagnola, and Y. Kawakatsu, "Extended Tisserand-Poincaré Graph and Multiple Lunar Swingby Design with Sun Perturbation," *Proceedings of the International Conference on Astrodynamics Tools and Techniques*, Darmstadt, Germany, March 14-17, 2016, 10 p.

[19] W. Kizner, "A Method of Describing Miss Distances for Lunar and Interplanetary Trajectories," *Planetary and Space Science*, Vol. 7, 1961, pp. 125–131.

[20] N. Strange, *Analytical Methods for Gravity-Assist Tour Design*. PhD thesis, Purdue University, 2016.

[21] N. Strange and J. Longuski, "Graphical Method for Gravity-Assist Trajectory Design," *Journal of Spacecraft and Rockets*, Vol. 39, No. 1, 2002, pp. 9–16.

[22] R. Russell and C. Ocampo, "Geometric Analysis of Free-Return Trajectories Following a Gravity-Assisted Flyby," *Journal of Spacecraft and Rockets*, Vol. 42, No. 1, 2005, pp. 138–152.

[23] N. Strange, R. Russell, and B. Buffington, "Mapping the V-infinity Globe," *Advances in the Astronautical Sciences*, Vol. 129, 2007, 24 p.

[24] A. Tselousova, M. Shirobokov, and S. Trofimov, "Geometrical Tools for the Systematic Design of Low-Energy Transfers in the Earth-Moon-Sun System," *Advances in the Astronautical Sciences*, Vol. 175, 2020, pp. 5233–5250.

[25] R. Castelli, "Regions of Prevalence in the Coupled Restricted Three-Body Problems Approximation," *Communications in Nonlinear Science and Numerical Simulation*, Vol. 17, No. 2, 2012, pp. 804–816.

[26] D. Okhotsimskii and Y. Sikharulidze, *Osnovy mekhaniki kosmicheskogo poleta (Fundamentals of Space Flight Mechanics)*. Moscow: Nauka, 1990.